Available online at www.sciencedirect.com
SCIENCE DIRECT®
International Journal of Heat and Fluid Flow 26 (2005) 334–347
International Journal of HEAT AND FLUID FLOW
www.elsevier.com/locate/ijhff

Impact of molten metal droplets on the tip of a pin projecting from a flat surface

R. Ghafouri Azar, Z. Yang, S. Chandra, J. Mostaghimi *

Department of Mechanical and Industrial Engineering, Centre for Advanced Coating Technologies, University of Toronto, 5 King's College Road, Toronto, Ont., Canada M5S 3G8

Received 20 March 2004; accepted 7 August 2004
Available online 18 October 2004

Abstract

We photographed impact of molten zinc and tin droplets on a flat steel surface from which the tip of a small pin was projecting. The height of the pin and its distance from the droplet center was varied. A three-dimensional model of droplet impact and solidification was used to predict splat shapes formed by droplets after they had spread and frozen. The model calculated velocity and pressure distributions in droplets and the growth of solid layers. When the offset distance of the pin was less than the droplet radius liquid flowed over the pin so that it had relatively little impact on the final splat shape. At larger offset distances a liquid sheet jetted from under the droplet after impact and impinged on the vertical surface of the pin. If the pin height was sufficiently large, approximately the same as the final splat thickness, it obstructed flow of liquid so that the solidified splat had a V-shaped notch in it. If pin height was made less than the average splat thickness liquid flowed over it and the final splat was circular, but the pin reduced flow velocity and suppressed growth of fingers along the edges of the splat that passed over the pin. Reduced velocities also resulted in faster growth of the solidified layer around the pin.

1. Introduction

The final shape assumed by a molten metal droplet after landing and freezing on a solid surface is of interest in many industrial applications such as spray coating, spray forming and solder jetting on circuit boards. Several numerical models have been developed to simulate fluid flow and heat transfer during droplet impact. Earlier models were two dimensional, making the assumption that droplets are symmetric about their vertical axis, which restricted their use to simulating normal impact on a flat surface (Trapaga and Szekely, 1991; Liu et al., 1993; Zhao et al., 1996; Waldvogel and Poulikakos, 1997; Attinger et al., 2000; Haferi and Poulikakos, 2002; Bertagnolli et al., 1997; Pasandideh-Fard et al., 1998). More recent three-dimensional codes have been used to model more complex flows such as impact on inclined surfaces (Bussmann et al., 1999; Pasandideh-Fard et al., 2002a), droplet break-up and splashing (Bussmann et al., 2000; Zheng and Zhang, 2000) and drop interactions (Ghafouri-Azar et al., 2003b).

Simulations have yielded considerable insight into the effect of fluid properties such as viscosity and surface tension on droplet deformation. The next major challenge in accurately modeling droplet impact lies in accurately characterizing surface properties. Most current models assume that droplets land on a perfectly flat, smooth substrate. Yet no real surface meets this definition and experiments have shown that even small irregularities in the surface, just a fraction of a micron in magnitude, may significantly affect impact dynamics (Shakeri and Chandra, 2002).

Protrusions on a surface can affect the motion of an impacting droplet in two different ways, depending on

* Corresponding author. Tel.: +1 416 978 5742; fax: +1 416 978 7753.
E-mail address: mostag@mie.utoronto.ca (J. Mostaghimi).

0142-727X/$ - see front matter © 2004 Elsevier Inc. All rights reserved.
doi:10.1016/j.ijheatfluidflow.2004.08.004

Nomenclature

C	specific heat
k	thermal conductivity
D	droplet diameter
D_{max}	maximum splat diameter
f	volume of fluid fraction
$\vec{F}_b$	body force
h	enthalpy
H_f	latent heat of fusion
L	offset distance
N	number of fingers around splat
p	pressure
q	heat flux
R_c	thermal contact resistance
T	temperature
t	time
u	velocity component in x-direction
T_m	melting temperature
T_w	substrate temperature
$\vec{V}$	velocity vector
w	velocity component in z-direction

Greeks

υ	kinematic viscosity
ρ	density
ϕ	energy equation source term
λ	liquid–solid volume fraction
β	energy equation enthalpy coefficient
δ	splat thickness

Non-dimensional parameters

Re	Reynolds number
We	Weber number

their size. If a droplet encounters a significant sized obstruction on a surface as it spreads liquid flow may be diverted, altering the splat shape. Fig. 1 shows examples of splats collected after plasma spraying nickel droplets (50–90 μm in diameter) at high velocity (~100 m/s) onto smooth stainless steel (Fig. 1a) or glass (Fig. 1b) plates. In both cases it is clear that that the drops encountered obstacles on the surface that diverted their outwards flow so that the splats are not circular, but have notches in them. Irregularities in the splat periphery have important practical consequences since they create voids in a coating, reducing its adhesion strength and structural integrity. Obstacles to flow are often created by debris from previously deposited drops. But even when a molten droplet lands on a perfectly clean surface its edges begin to freeze immediately after impact. If solidification is sufficiently rapid frozen portions of the rim become large enough to impede flow (Pasandideh-Fard et al., 2002b).

Small asperities, usually classified as surface roughness, are too small to present a barrier to flow, but produce random perturbations in flow velocity. Instabilities generated around the rim of a spreading by velocity fluctuations are amplified as the droplet spreads, leading to

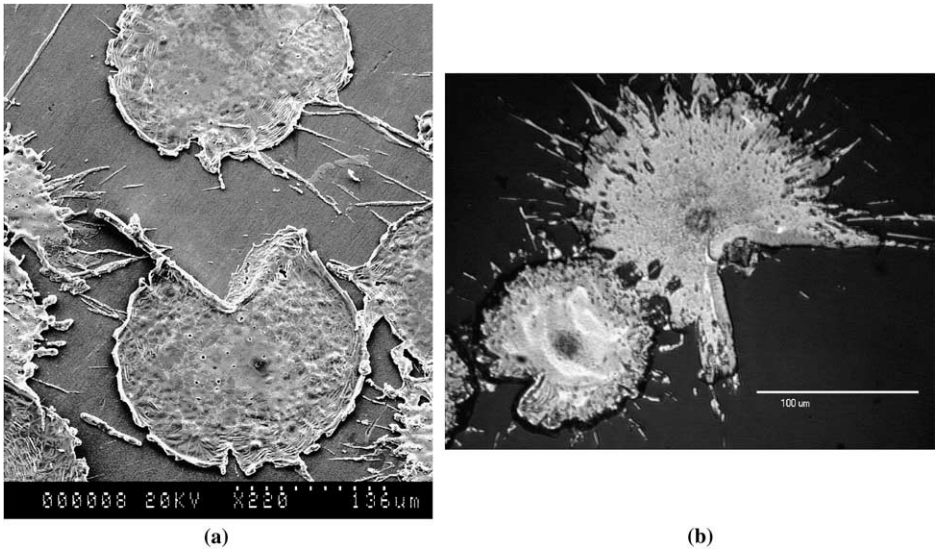

Fig. 1. Splats collected after plasma spraying nickel droplets (50–90 μm in diameter) at high velocity (~100 m/s) onto (a) a stainless steel surface (viewed from above) and (b) a glass surface (viewed from below).

the growth of fingers around its edge (Bussmann et al., 2000; Kim et al., 2000).

How large does an obstruction have to be for it to obstruct flow? The answer is not obvious. Experiments with molten metal droplets landing on grit blasted surfaces showed that small variations in roughness produced large changes in impact dynamics (Shakeri and Chandra, 2002). But interpretation of those results is complicated by the fact that greater surface roughness also enhances thermal contact resistance between the droplet and substrate, reducing heat transfer. It is difficult to isolate the effects of surface roughness on fluid flow when dealing with molten metal drops.

Surface features are typically several orders of magnitude smaller than droplets, making it prohibitively time consuming to generate a computational mesh fine enough to accurately describe a real surface. Simulations of droplet impact on rough surfaces have attempted to model surface irregularities as a series of concentric, evenly spaced ridges with sinusoidal profiles (Liu et al., 1995). It is not clear, though, how realistic such a representation is.

Our efforts to model droplet impact are part of a program to simulate formation of coatings (Ghafouri-Azar et al., 2003a) by a spray of molten droplets hitting a surface. We have used a three-dimensional code to simulate droplet deformation and solidification (Pasandideh-Fard et al., 2002a), and to study interactions between droplets landing on a surface (Ghafouri-Azar et al., 2003b). We intend, next, to incorporate more realistic droplets–surface interactions. Before doing that we need a better understanding of how small obstacles on a surface affect droplet impact, and to confirm that we can accurately simulate interactions between an impacting drop and surface features.

The objective of the present study were to (a) photograph impact of molten zinc and tin droplets on a stainless steel plate which had the tip of a small pin projecting above it; (b) observe the effect of varying both the height of the pin and the distance between the droplet and pin centers on droplet impact dynamics and determine conditions under which the pin would obstruct flow; and (c) validate use of a numerical model in simulating interactions between impinging molten metal drops and the pin projecting out of the substrate.

2. Experimental method

The method of generating molten metal droplets and photographing their impact has been described in detail earlier (Ghafouri-Azar et al., 2003b; Shakeri and Chandra, 2002; Aziz and Chandra, 2000). Droplets of molten zinc and tin were produced and released in free fall onto a stainless steel plate that had the tip of a pin projecting above it. A pneumatic droplet generator (Shakeri and Chandra, 2002; Cheng and Chandra, 2003) was used to force molten metal droplets out of a nozzle by applying pulses of nitrogen. A synthetic sapphire nozzle with a 0.46 mm diameter orifice was used to produce 2.7 mm zinc droplets and 2.5 mm tin droplets. A droplet generator made of stainless steel was used to produce tin droplets (99.8% pure Aldrich Chemical Co., Milwaukee, WI.). To contain molten zinc (99.9% pure, TeckCominco Inc., Mississauga, Ontario), which is highly reactive, the droplet generator body was machined from graphite. The temperature of the droplet generator was held at 450 °C when working with zinc (melting point 420 °C) and at 250 °C when working with tin (melting point 232 °C).

Droplets fell through a heated 25.4 mm diameter aluminum tube onto the test surface. To prevent oxidation of droplets nitrogen was continuously blown through two holes in the tube wall near the nozzle. The distance between the nozzle and the test surface was 0.511 m, giving an impact velocity of 3.18 m/s. Calculations of heat loss during the fall of droplet (Yang, 2002) showed that its temperature of zinc drops was 438 °C just before impact and that of tin drops was 240 °C.

The test chamber housing the stainless steel substrate was made of aluminum with a plastic window in front to allow viewing. The test surface on which droplets impinged was a 50.8 mm square by 6.35 thick stainless steel plate polished with 1500 grit emery cloth to an average roughness of 0.07. A 0.6 mm diameter stainless steel pin was inserted vertically through a hole drilled in the plate, its height above the surface adjusted with a feeler gauge (to either 0.25 mm, 0.35 mm, or 0.5 mm) and then locked in place by tightening a bolt inserted into the side of the plate. The test plate was mounted on a translation stage and moved horizontally to vary the distance between the centers of the pin and droplet. The plate was kept at room temperature (≈25 °C) prior to depositing a droplet on it.

Droplet impact was photographed using a single shot flash photographic method (Ghafouri-Azar et al., 2003b; Shakeri and Chandra, 2002; Aziz and Chandra, 2000). A Nikon E3 digital camera was used to take a single 8 μs flash photograph of an impacting drop. An entire impact sequence was obtained by photographing different droplets at different stages of impact.

3. Numerical method

The numerical code used to model the spreading and solidification of droplets was the same described earlier by Pasandideh-Fard et al. (2002a) and Ghafouri-Azar et al. (2003b). The code simultaneously solves equations of mass and momentum and energy discretized using a finite volume technique on a 3-D Eulerian structured

grid. The volume-of-fluid (VOF) algorithm is used for tracking the free surface of the droplet and the solid layer in it. The volume-of-fluid (f), is defined as the fraction of a cell volume occupied by fluid and equals one for a cell full of fluid, zero for an empty cell, and a fraction between zero and one for a free surface cell. Advection of the volume-of-fluid is governed by the equation

$$\frac{\partial f}{\partial t} + (\vec{V} \cdot \vec{\nabla}) f = 0, \tag{1}$$

where $\vec{V}$ represents the velocity vector and t the time. To identify and track the solid phase a second liquid volume fraction (λ) is defined as a parameter whose value is equal to one in the liquid and zero in the solid and a fraction in cells at the liquid–solid interface. In locations where both liquid and solid phases exist, the liquid phase has volume fraction λ, and the solid phase $(1-\lambda)$, in which the liquid portion (λ) is free to flow while the remaining portion $(1-\lambda)$ is frozen. To account for solidification the advection equation is modified to

$$\frac{\partial f}{\partial t} + (\lambda \vec{V} \cdot \vec{\nabla}) f = 0. \tag{2}$$

The method of solving conservation equations in cells with both liquid and solid is the same as those used for cells with no solid, except that solidified region are treated as a liquid with zero velocity.

Having defined the new volume fraction for solid cells, the conservation equations of mass and momentum are written as

$$\vec{\nabla} \cdot (\lambda \vec{V}) = 0, \tag{3}$$

$$\frac{\partial (\lambda \vec{V})}{\partial t} + (\lambda \vec{V} \cdot \vec{\nabla}) \vec{V} = \frac{-\lambda}{\rho} \vec{\nabla} p + \lambda \upsilon \nabla^2 \vec{V} + \frac{\lambda}{\rho} \vec{F}_{\mathrm{b}}, \tag{4}$$

where υ is the kinematic viscosity, is the density p is the pressure, and $\vec{F}_{\mathrm{b}}$ is any body forces that act on the fluid. Surface tension was considered to be a component of the body force acting on the fluid free surface. Fluid flow was assumed to be Newtonian, laminar and incompressible. Any effect of the ambient air on the droplet evolution was neglected. Only normal stresses were assumed to act on the free surface. Laplace's equation was used to determine the pressure at the free surface.

The conservation of energy equation combined with the enthalpy-transforming model (Cao et al., 1989) was used to model heat transfer. Assuming that the phase change occurs at a single temperature, the temperature (T) is related to enthalpy (h) by

$$T = T_{\mathrm{m}} + \frac{1}{k}(\beta h + \phi), \tag{5}$$

where T_{m} is the melting point and k is the thermal conductivity. Depending on the state of fluid, the coefficients β and ϕ can be defined as

$$\begin{cases} \beta = \frac{k_{\mathrm{s}}}{C_{\mathrm{s}}} \text{ and } \phi = 0 & h \leqslant 0 \text{ (solid phase)}, \\ \beta = 0 \text{ and } \phi = 0 & 0 < h < H_{\mathrm{f}} \text{ (liquidsolid interface)}, \\ \beta = \frac{k_{\mathrm{l}}}{C_{\mathrm{l}}} \text{ and } \phi = \frac{-H_{\mathrm{f}} k_{\mathrm{l}}}{C_{\mathrm{l}}} & h \geqslant H_{\mathrm{f}} \text{ (liquid phase)}, \end{cases} \tag{6}$$

where C represents the specific heat, h the enthalpy and H_{f} the heat of fusion. The energy equation becomes:

$$\rho \frac{\partial h}{\partial t} + \rho (\vec{V} \cdot \vec{\nabla}) h = \nabla^2 (\beta h) + \nabla^2 \phi. \tag{7}$$

No-slip and no-penetration boundary condition were applied at solid surfaces. Liquid–solid contact angles were prescribed (Bussmann et al., 1999) with advancing and receding contact angles for tin on stainless steel set at 140° and 40°, respectively (based on measurements by Aziz and Chandra, 2000). The dynamic contact angle between liquid tin and solid tin was assumed to be 90°.

Free surfaces of droplets and exposed portions of the substrate were assumed adiabatic. Heat flux (q) at the droplet–substrate interface was calculated using

$$q = \frac{T - T_{\mathrm{w}}}{R_{\mathrm{c}}}, \tag{8}$$

where R_{c} is the thermal contact resistance and T_{w} the substrate temperature. A value of $R_{\mathrm{c}} = 4 \times 10^{-5}\,\mathrm{m^2 K/W}$ was used at all interfaces in the model. Properties of molten droplets (Incropera and DeWitt, 1990; Boyer and Gall, 1995) were assumed to be constant, but substrate thermal properties were allowed to vary with temperature.

The procedure for solving the governing equations has been described by Ghafouri-Azar et al. (2003b). Simulations were carried out on a Linux 2.4.16-cluster-996 machine using a mesh that had uniform grid spacing in the x-, y- and z-directions, equal to 22 cells per radius of the impacting droplets. Mesh refinement studies (Bussmann et al., 1999) have shown that at this resolution predicted droplet shapes and the evolution of splat diameter are independent of grid size. Symmetry about the plane passing through the droplet and pin centers allowed us to confine our calculation domain to half of the droplet. Typical CPU times for simulating droplet impact were about 3–4 days. The maximum Courant number used in the simulations was 0.65.

4. Results

Fig. 2 shows 2.7 mm diameter zinc droplets that landed with a velocity of 3.18 m/s on a 0.6 mm diameter stainless steel pin (height h = 0.35 mm) with different offset distances (L = 5.7 mm, 0.65 mm, 1.25 mm and 2.50 mm) between droplet and pin centers. Droplet temperature just before impact was 438 °C. Photographs were taken of splats formed by droplets after they had spread and solidified. With L = 5.7 mm (see Fig. 2a)

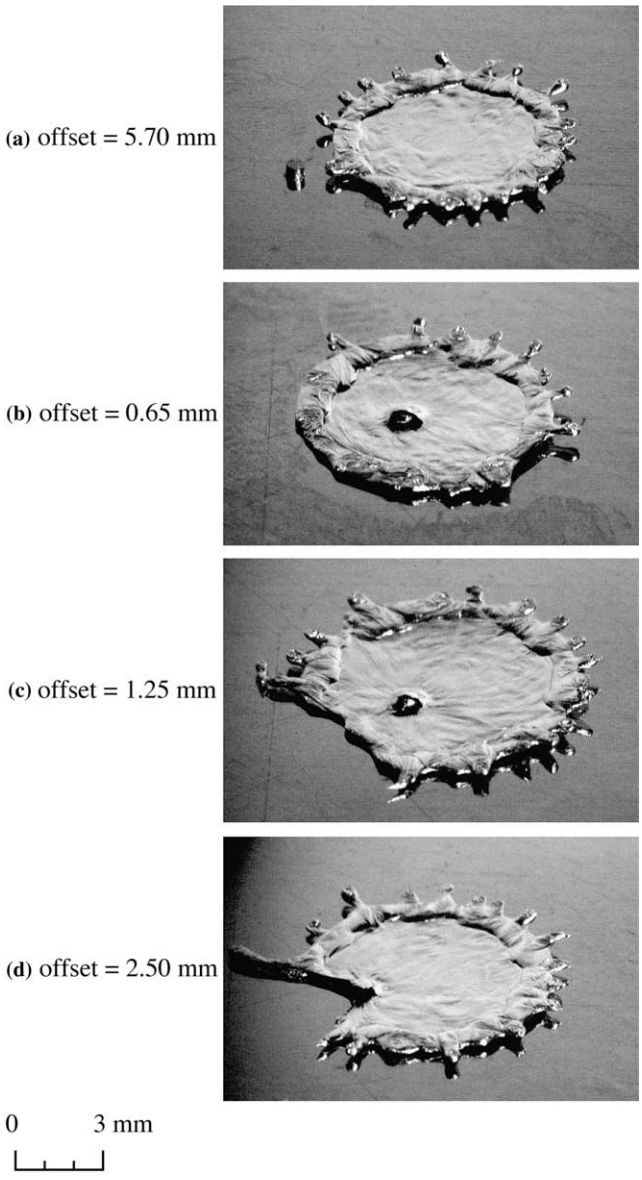

Fig. 2. Splats formed by impact and solidification of zinc droplets (diameter 2.7 mm, velocity 3.18 m/s) on a stainless steel surface at 25 °C with a 0.35 mm high, 0.6 mm diameter pin protruding at a distance of (a) 5.70 mm, (b) 0.65 mm, (c)1.25 mm and (d) 2.50 mm from the droplet center.

the droplet did not touch the pin at all. The final splat was circular with fingers spaced evenly around its edge. Mehdizadeh (2003) proposed a simple relation to predict the number of fingers (N) that develop around a liquid drop at its maximum extension, based on a Rayleigh–Taylor instability analysis (Kim et al., 2000):

$$N = 1.14We^{0.5}. \tag{9}$$

For the impact conditions of Fig. 2 $We = 230$ and $Re = 1.6 \times 10^4$, giving $N = 17$. A count of the number of fingers around the splat in Fig. 2a yields $N = 18$.

When the offset distance was reduced to 0.65 mm (Fig. 2b) the center of the pin was approximately half a radius away from the droplet center and the droplet covered it almost immediately after impact. In this case the edge of the splat was again circular, but there were no fingers on the side of the splat that first encountered the pin. The pin appeared to inhibit growth of fingers as it slowed down the liquid flowing over it.

With the pin placed at an offset distance equal to the droplet radius (Fig. 2c, $L = 1.25$ mm) the edge of the splat became straight. There were no fingers along the straight segment, while the two fingers at either end of it were longer than the others. Finally, with $L = 2.5$ mm the pin was positioned far enough from the droplet center that liquid did not reach it until fairly late during droplet spread. Flow was diverted to either side of the pin so that the splat had a V-shaped gap in it with long fingers on either side. The final splat (Fig. 2d) resembles those seen in Fig. 1.

Information about the dynamics of droplet impact on the tip of the pin can be obtained from photographs showing different stages of droplet deformation. Fig. 3 shows the impact of 2.5 mm tin droplets landing with a velocity of 3.18 m/s beside a stainless steel pin. Each frame shows successive stages of droplet impact and the time from the instant of impact is indicated. The offset distance (L) between pin and droplet centers was so large that the droplet did not touch the pin while spreading. The droplet landed on the stainless steel substrate, spread to its maximum extent and completely solidified. Twenty-four evenly distributed fingers were formed around the periphery of the splat. For the impact conditions $We = 325$ and $Re = 2.9 \times 10^4$; Eq. 9 predicts 21 fingers.

In the photographs shown in Fig. 4 the pin was moved closer to the droplet center. Two impact sequences are shown, for offset distances of (a) $L = 1.4$ mm, which was just slightly larger than the droplet radius and (b) $L = 2.0$ mm. The pin height (h) was kept at 0.25 mm. Experiments showed that a pin with height less than this had almost no discernible effect on splats. The average thickness (δ) of a splat, assuming that it is a cylinder with diameter D_{max}, can be calculated by equating its volume to that of the spherical droplet, giving

$$\delta = \frac{2}{3}\frac{D^3}{D_{max}^2}. \tag{10}$$

From Eq. (10), the splats in Figs. 3 and 4 have a thickness of approximately 0.2 mm; the pin height has to be of the same order of magnitude for it to affect flow.

At the lower offset distance (see Fig. 4a, $L = 1.4$ mm) the liquid touched the pin by the first frame ($t = 0.2$ ms), flowed over it so that the pin was com-

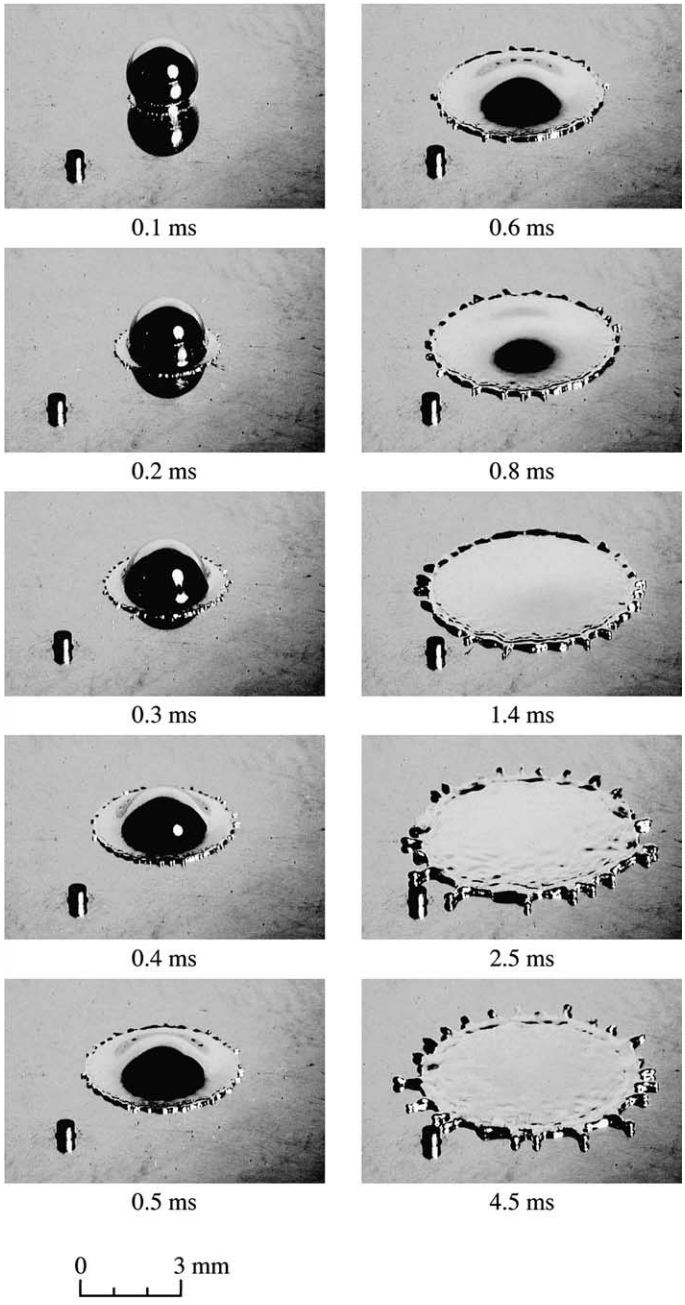

Fig. 3. Impact of a 2.5 mm diameter molten tin droplet with velocity 318 m/s on a stainless steel surface at 25 °C.

pletely covered ($t = 0.4$ ms), and continued to spread out. After the droplet had flattened out the tip of the pin could be seen protruding through the splat ($t = 2.5$ ms). When the offset distance was increased to $L = 2.0$ mm (Fig. 4b) the droplet edge first contacted the pin at $t = 0.4$ ms. The pin appeared to promote finger formation; two long fingers formed on either side of the pin ($t = 0.6$ ms). The final splat ($t = 2.5$ ms) had no finger in the radial direction from its center along which the pin lay.

Doubling the height of the pin produced much greater effects on the splat shape. Fig. 5 shows two sequences of photographs of tin droplets landing on a 0.5 mm high pin. With 1.4 mm offset (Fig. 5a) the side of the droplet touched the pin almost immediately after impact so that liquid jetted over the top of pin ($t = 0.2$–0.4 ms). The final splat ($t = 4.5$ ms) had an almost straight edge where it hit the pin, with a single short finger in the center produced by the liquid passing over the pin and two large fingers on either end. Perturbation of the flow by the pin also appeared to increase the size of fingers (compare with Figs. 3 and 4). When the offset was increased to 2.0 mm (Fig. 5b) liquid did not touch the pin until after $t = 0.4$ ms. First contact with the pin was made

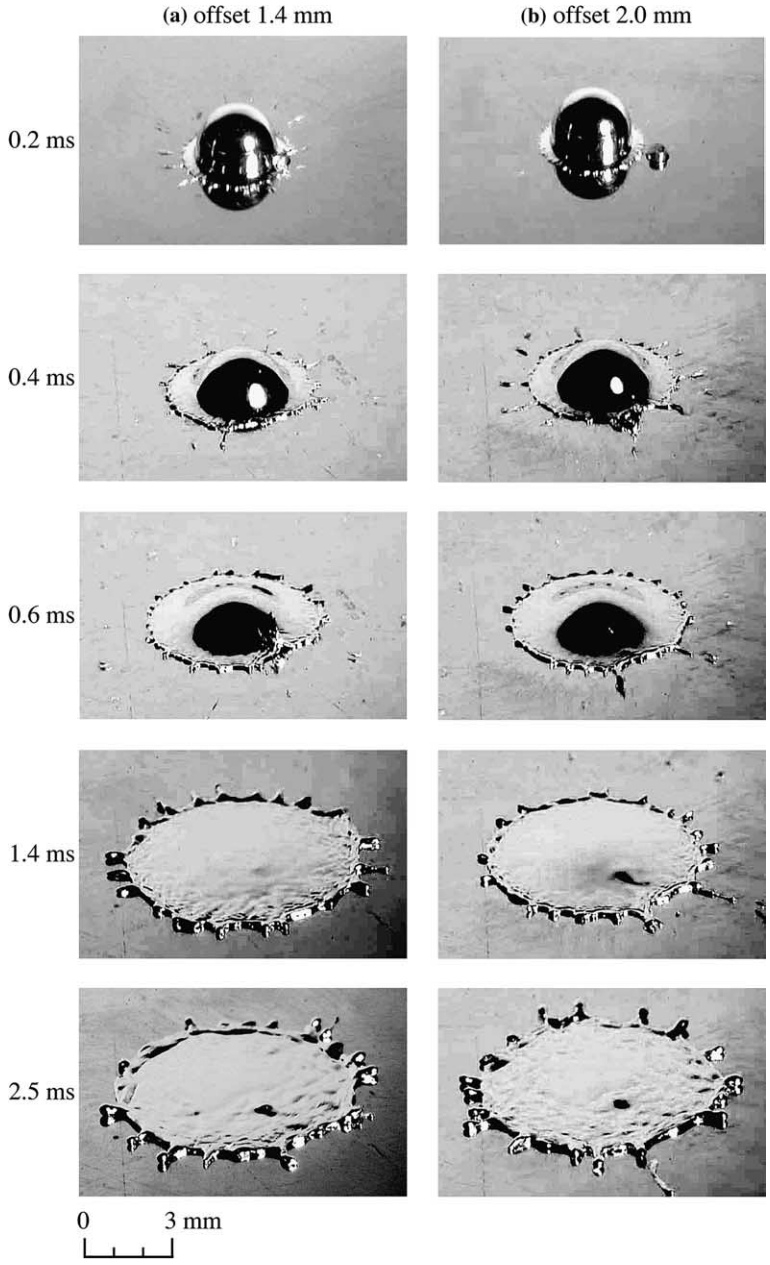

Fig. 4. Impact of tin droplets (diameter 2.5 mm, velocity 3.18 m/s) on a stainless steel surface at 25 °C with a 0.25 mm high pin protruding at a distance of (a) 1.4 mm and (b) 2.0 mm from the droplet center.

by the thin sheet of liquid jetting out from under the drop rather than the side of the drop. The advancing liquid sheet could not surmount the pin, but was instead diverted around the pin forming a V- shaped gap with long fingers on either side. The final splat shapes ($t = 4.5$ ms) resemble the nickel and zinc splats seen in Figs. 1 and 2.

Photographs alone do not give details of velocity distributions in droplets or the location of the solidification front. We therefore used a three-dimensional numerical model to simulate droplet impact. Fig. 6 shows a comparison between photographs and computer generated images of droplets landing on a surface with a projecting pin. Photographs are shown in the left column and corresponding predicted droplet shapes, at the same time after impact, on the right. Pin height was kept at 0.35 mm, approximately midway between those in Figs. 4 and 5, and offset distance $L = 1.4$ mm. The liquid collided with the pin by 0.2 ms and was diverted on either side of it, while a finger of liquid passed over the top of the pin ($t = 0.4$ ms). Liquid passing on either side of the pin completely surrounded it ($t = 1.2$ ms). The pin reduced the velocity of liquid passing over it so that the final splat was asymmetrical, flattened on the side

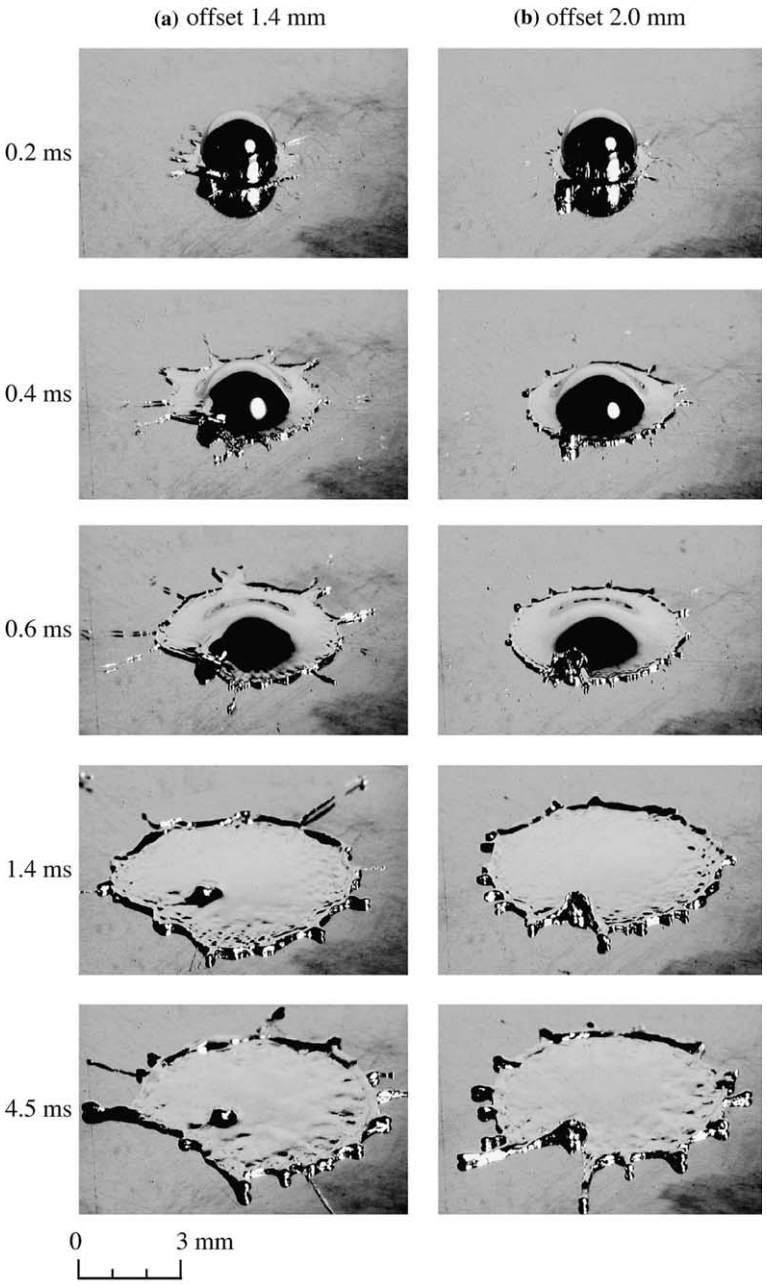

Fig. 5. Impact of tin droplets (diameter 2.5 mm, velocity 3.18 m/s) on a stainless steel surface at 25 °C with a 0.50 mm high pin protruding at a distance of (a) 1.4 mm and (b) 2.0 mm from the droplet center.

towards the pin ($t = 2.4$ ms). A single finger produced by the liquid jetting over the pin is visible in both photographs and simulations.

Small fingers are visible around splat edges in both photographs and simulations, produced by instabilities due to small velocity fluctuations at the leading edge of the fluid (Kim et al., 2000). In experiments these are caused by variations in surface properties and increase in magnitude with surface roughness. They can be reproduced in simulations by artificially perturbing the liquid velocity after impact (Bussmann et al., 2000); small variations in initial velocity result in growth of fingers as the droplet spreads. When the droplet simultaneously freezes as it spreads, solidification itself produces localized variations in the velocity field and triggers formation of fingers. These are clearly visible in Fig. 6, where fingers are prominent on the side of the splat opposite to the pin. The pin reduced the velocity of liquid flowing over it and suppressed growth of fingers, except for the single finger in line with it (see $t = 2.4$ ms).

Fig. 7 shows photographs and simulations under the same conditions as Fig. 6, except that the offset distance

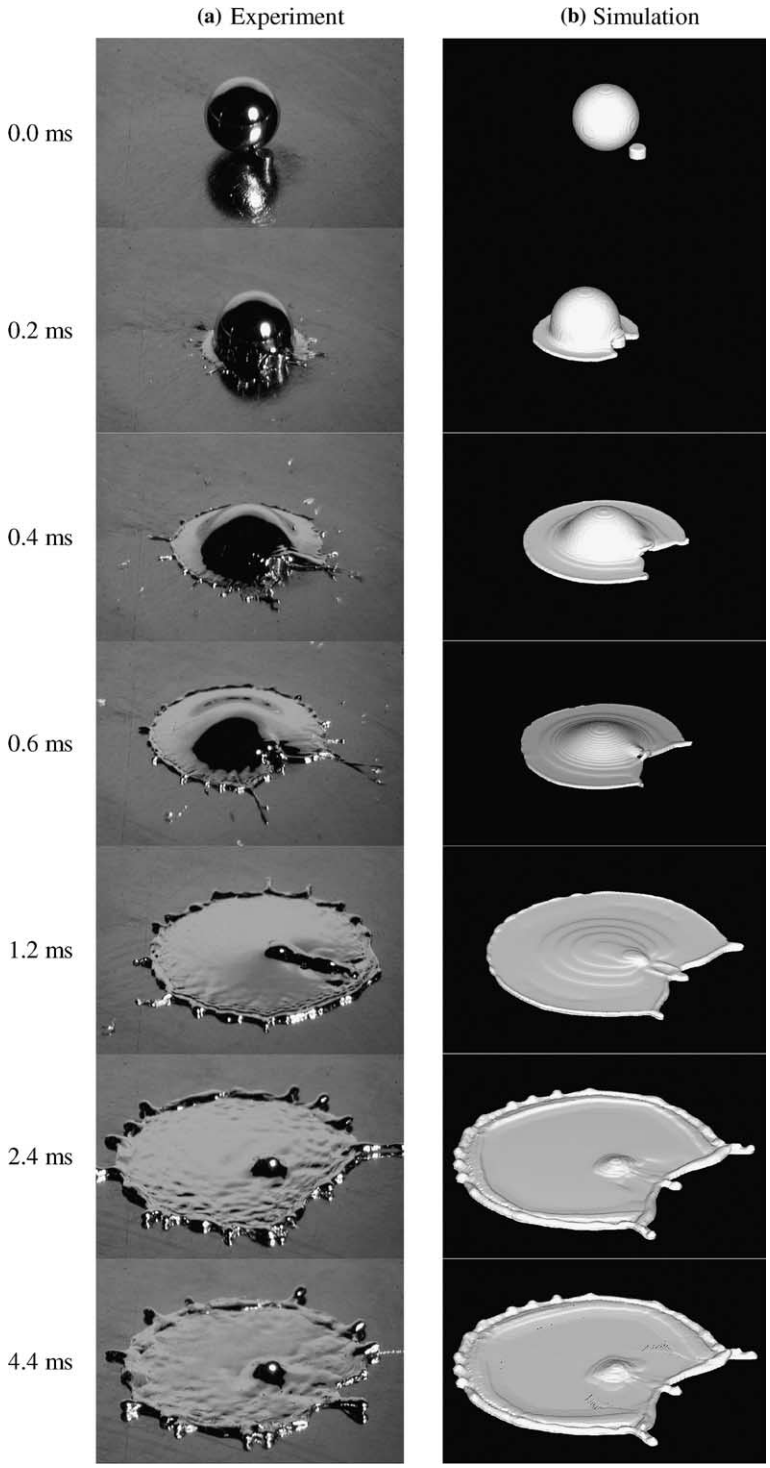

Fig. 6. Comparison of photographs and computer generated images of a 2.5 mm diameter tin droplet landing with a velocity of 3.18 m/s at a point 1.4 mm from the center of a 0.6 mm diameter pin with 0.35 mm height.

was increased to $L = 2.0$ mm. In this case the liquid did not surmount the pin. Instead the liquid flow parted to form two long strands that did not rejoin downstream but continued to flow away from each other in directions tangential to the pin. The resulting splat had the distinctive V-shaped gap seen in Fig. 1. There were small fingers around the splat edge on the side away from the pin.

Why does a small change in offset distance affects splat shape so much? To understand this it helps to look at the growth of the solid layer in the splat. Fig. 8 shows the evolution of splat shape from simulations, with the

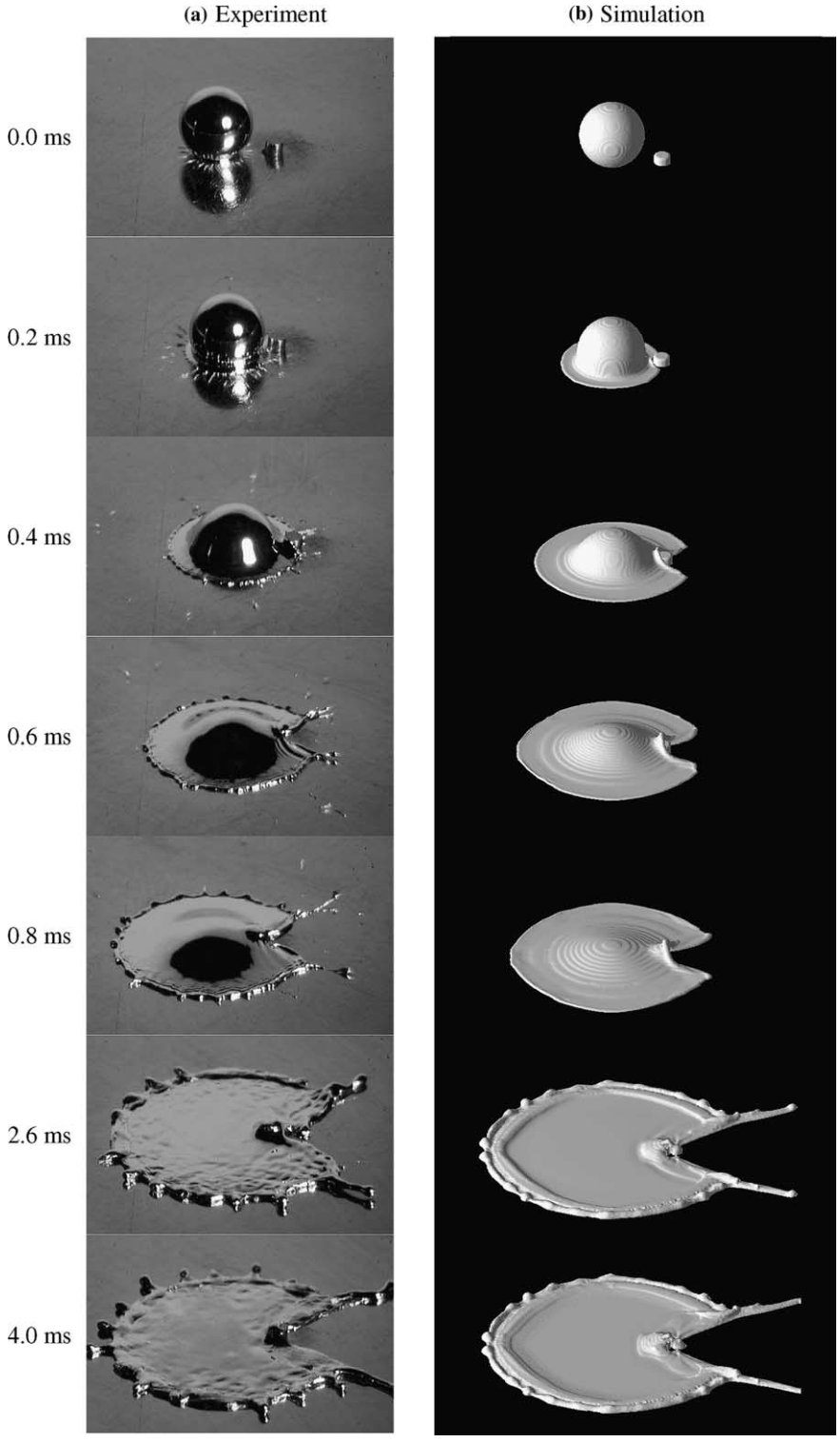

Fig. 7. Comparison of photographs and computer generated images of a 2.5 mm diameter tin droplet landing with a velocity of 3.18 m/s at a point 2.0 mm from the center of a 0.6 mm diameter pin with 0.35 mm height.

liquid rendered transparent and solid portions shown as a dark grey. Impact on pins at both offset distances, 1.4 and 2.0 mm, are shown. Solidification started around the edges of splats where liquid first contacted the colder substrate. By $t = 0.6$ ms the drop with $L = 2.0$ mm had a solid ridge around the entire splat periphery, whereas with $L = 1.4$ mm solidification was not complete and the liquid completely engulfed the pin. Solidification

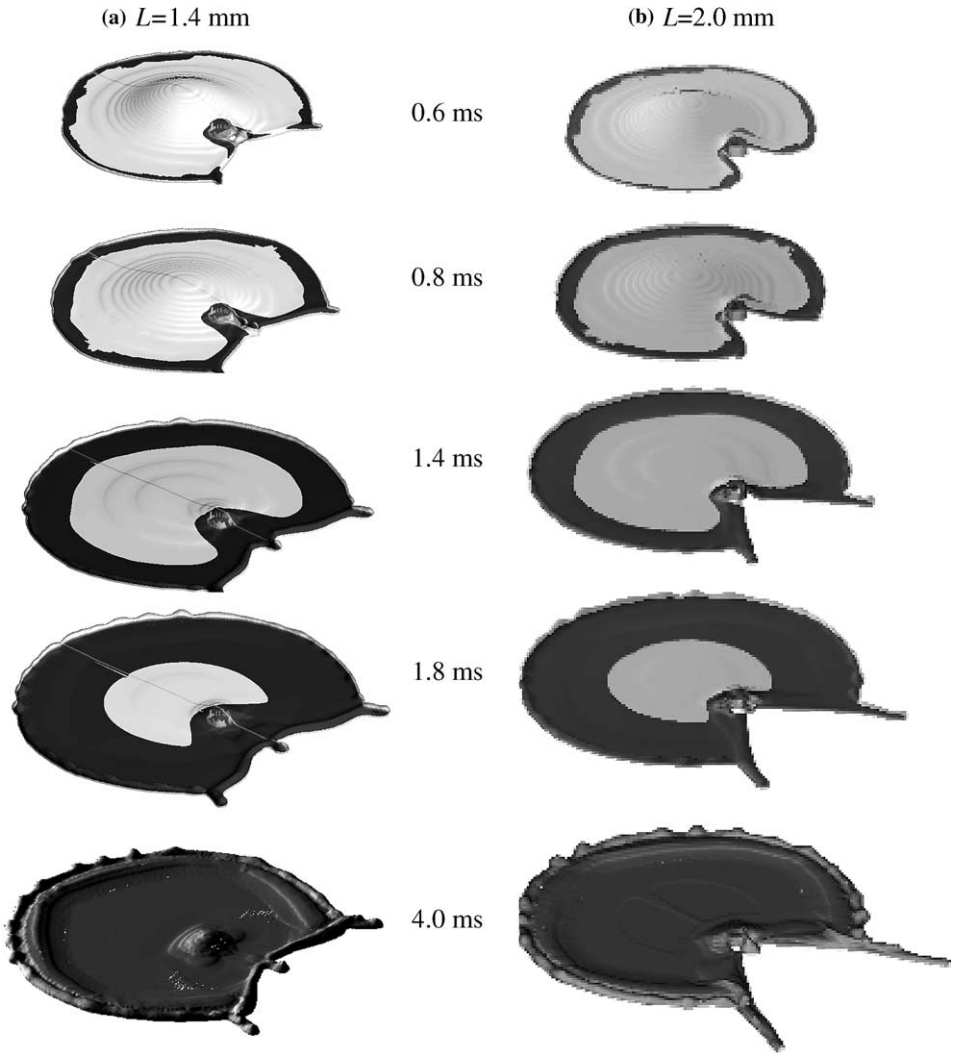

Fig. 8. Growth of solid layer in 2.5 mm diameter tin droplets landing with a velocity of 3.18 m/s on a stainless steel surface at a point (a) 1.4 mm and (b) 2.0 mm from the center of a 0.35 mm high pin.

progressed faster in the region around the pin, especially in its wake, since liquid velocities were lower there and the supply of hot liquid flowing out of the bulk of the droplet was reduced. The liquid had lower momentum after it bypassed the pin at $L = 2.0$ mm and did not surmount the frozen rim but was diverted by it, creating two long fingers. The solid layer grew towards the center of the splat which was completely frozen by $t = 4.0$ ms.

Fig. 9 shows cross-sections through impacting droplets, in a plane passing through the centers of both pin and droplet. Arrows indicate velocity vectors and lines constant pressure contours. At three representative points in each frame values are given of u and w, the velocity components in the x- and z-directions, and liquid pressure p. The left column shows successive stages of impact on a pin with height 0.35 mm with its center offset by $L = 1.4$ mm from the droplet center. The droplet radius was 1.25 ms, so that it overlapped the edge of the pin at impact. At $t = 0.1$ ms liquid in the interior of the drop was still moving at near initial droplet velocity, and had already partially covered the pin. High pressures ($p > 22$ kPa at $t = 0.1$ ms, increasing to more than 42 kPa by $t = 0.3$ ms) were produced where liquid collided directly with the vertical surface of the pin. This high-pressure region drove liquid horizontally over the top of the pin with enough velocity ($u > 2$ m/s at $t = 0.4$ ms) for it to continue jetting outwards and form the single finger seen in Fig. 6.

When offset distance was increased to $L = 2.0$ mm the droplet did not cover the pin during impact (see Fig. 9b at $t = 0.1$ ms). A thin sheet of liquid, smaller than the height of the pin, jetted out from under the droplet after impact. When this liquid collided with the pin large stagnation pressures were generated ($p > 86$ kPa at $t =$

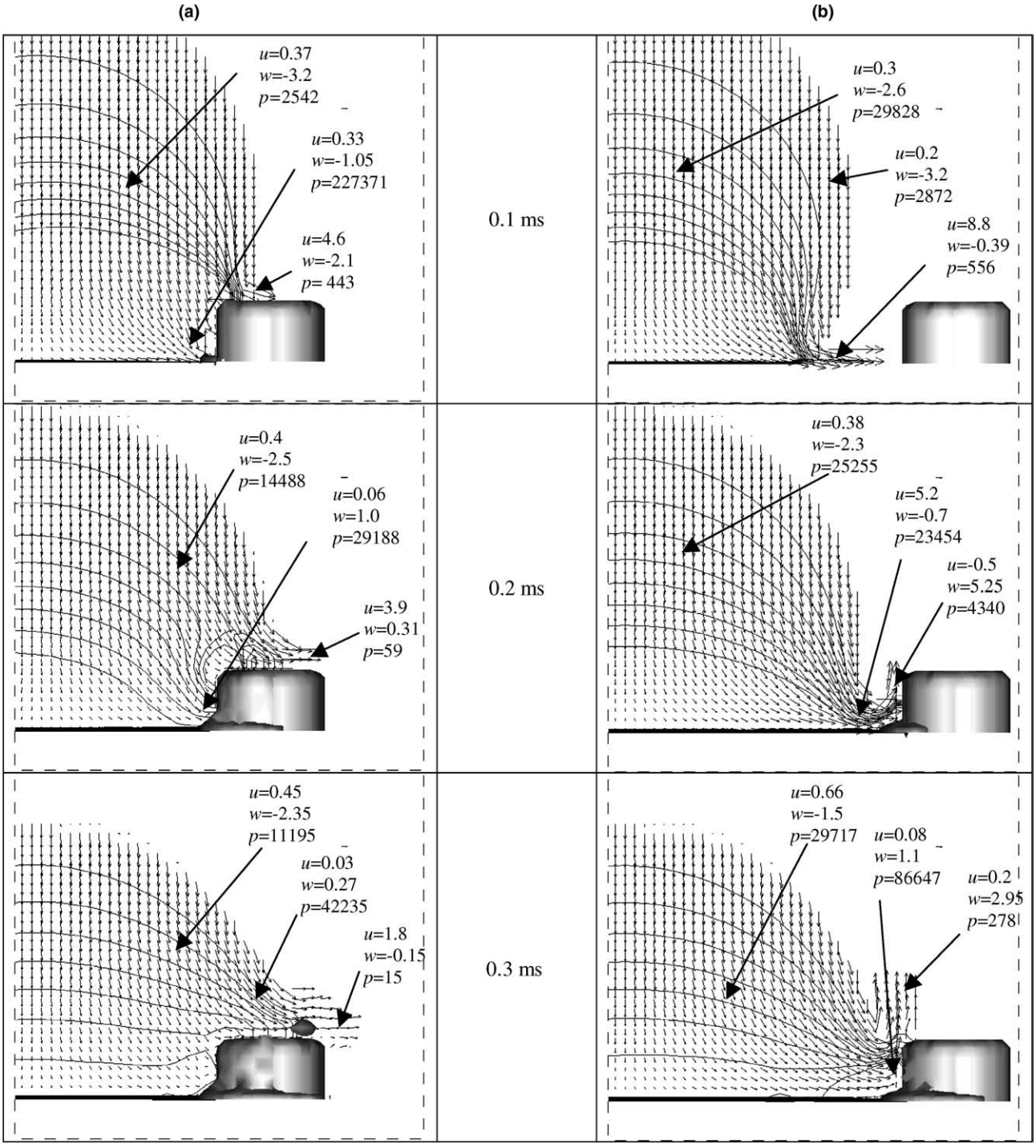

Fig. 9. Velocity and pressure distributions within 2.5 mm molten tin droplets impacting on a 0.35 mm high pin at an offset distance of (a) $L = 1.4$ mm and (b) $L = 2.0$ mm. Arrows indicate velocity vectors and lines pressure contours. u and w are velocity components in the x- and z-direction with units of metre per second and p is pressure in Pascal.

0.3 ms). This pressure forced liquid to rise up along the vertical face of the pin. By the time this liquid fell back onto the top of the pin pressure in the droplet had dissipated (see $t = 0.6$ ms) and liquid flowing over the pin traveled only a short distance producing the V-shaped gap seen in the splat in Fig. 7.

5. Summary and conclusions

Impact of molten zinc and tin droplets on a surface with the tip of a small pin projecting from it was photographed. A three-dimensional model of droplet impact and solidification was able to predict splat shapes, and

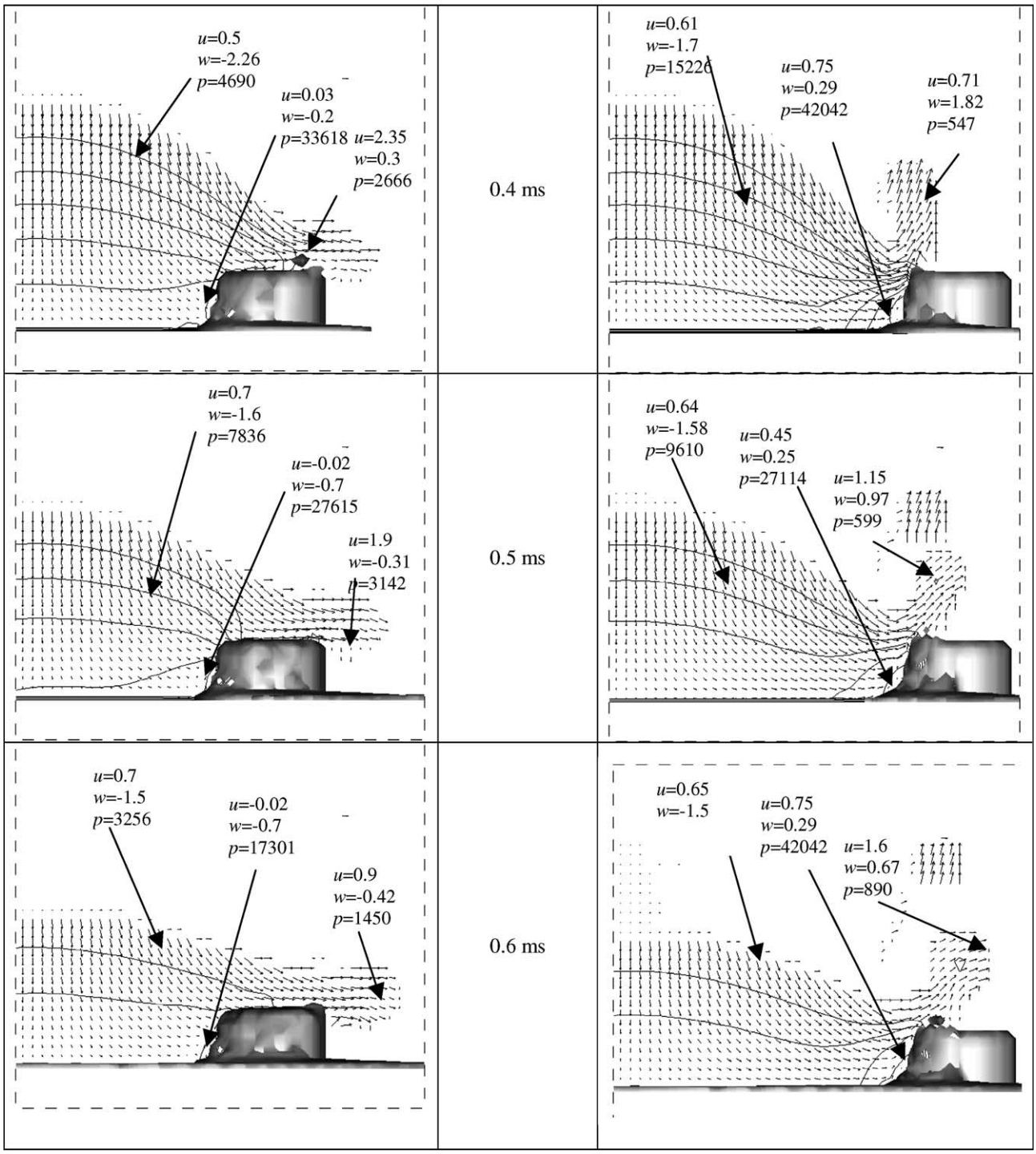

Fig. 9 (*continued*)

their variation with distance between droplet and pin centers, quite accurately. The model was used to calculate velocity and pressure distributions in droplets and the location of the solid layer.

When the offset distance of the pin was less than the droplet radius liquid covered the pin immediately after impact and flowed over it so that the obstruction had relatively little impact on the final splat shape. At larger offset distances a liquid sheet jetting from under the droplet impinged on the pin after impact. If the pin height was sufficiently large, approximately the same as the final splat thickness, it obstructed flow of liquid so that the solidified splat had a V-shaped notch in it. If pin height was decreased liquid flowed over it and the final splat was circular, but the pin reduced flow velocity and suppressed growth of fingers along the edges of the splat that

passed over the pin. Reduced velocities also resulted in faster growth of the solidified layer around the pin.

Acknowledgements

This research was supported by the Natural Sciences and Engineering Research Council of Canada, Materials and Manufacturing Ontario and members companies of the Centre for Advanced Coating Technologies at the University of Toronto.

References

Attinger, D., Zhao, Z., Poulikakos, D., 2000. An experimental study of molten microdroplet surface deposition and solidification: transient behavior and wetting angle dynamics. Journal of Heat Transfer 122, 544–556.

Aziz, S., Chandra, S., 2000. Impact, recoil and splashing of molten metal droplets. International Journal of Heat and Mass Transfer 43 (16), 2841–2857.

Bertagnolli, M., Marchese, M., Jacucci, G., Doltsinis, I.St., Noelting, S., 1997. Thermomechanical simulation of the splashing of ceramic droplets on a rigid substrate. Journal of Computational Physics 133, 205–221.

Boyer, H.E., Gall, T.L., 1995. Metals Handbook, Desk ed. American Society for Metals, Metals Park, Ohio.

Bussmann, M., Mostaghimi, J., Chandra, S., 1999. On a three-dimensional volume tracking model of droplet impact. Physics of Fluids 11, 1406–1417.

Bussmann, M., Mostaghimi, J., Chandra, S., 2000. Modeling the splash of a droplet impacting on a solid surface. Physics of Fluids 12 (12), 3121–3132.

Cao, Y., Faghri, A., Chang, W.S., 1989. A numerical analysis of Stefan problems for generalized multi-dimensional phase-change structures using the enthalpy transforming model. International Journal of Heat and Mass Transfer 32, 1289–1298.

Cheng, S., Chandra, S., 2003. A pneumatic droplet-on-demand generator. Experiments in Fluids 34, 755–762.

Ghafouri-Azar, R., Mostaghimi, J., Chandra, S., Charmchi, M., 2003a. A stochastic model to simulate formation of a thermal spray coating. Journal of Thermal Spray Technology 12 (1), 53–69.

Ghafouri-Azar, R., Shakeri, S., Chandra, S., Mostaghimi, J., 2003b. Interactions between molten droplets impinging on a solid surface. International Journal of Heat and Mass Transfer 46, 1395–1407.

Haferi, S., Poulikakos, D., 2002. Transport and solidification phenomena in molten microdroplet pileup. Journal of Applied Physics 92, 1675–1689.

Incropera, F.P., DeWitt, D.P., 1990. Fundamentals of Heat and Mass Transfer, 3rd ed. John Wiley & Sons, New York.

Kim, H.Y., Feng, Z.C., Chun, J.H., 2000. Instability of a liquid jet emerging from a droplet upon collision with a solid surface. Physics of Fluids 12, 531–541.

Liu, H., Lavernia, E.J., Rangel, R., 1993. Numerical simulation of substrate impact and freezing of droplets in plasma spray processes. Journal of Physics D Applied Physics 26, 1900–1908.

Liu, H., Lavernia, E.J., Rangel, R.H., 1995. Modeling of molten droplet impingement on a non-flat surface. Acta Metallurgica Et Materialia 43, 2053–2072.

Mehdizadeh, N., 2003. Droplet impact dynamics: Effect of varying substrate temperature, roughness and droplet velocity, Ph.D. Thesis, University of Toronto.

Pasandideh-Fard, M., Bhola, R., Chandra, S., Mostaghimi, J., 1998. Deposition of tin droplets on a steel plate: simulations and experiment. International Journal of Heat and Mass Transfer 41, 2929–2945.

Pasandideh-Fard, M., Chandra, S., Mostaghimi, J., 2002a. A three-dimensional model of droplet impact and solidification. International Journal of Heat and Mass Transfer 45, 2229–2242.

Pasandideh-Fard, M., Pershin, V., Chandra, S., Mostaghimi, J., 2002b. Splat shapes in a thermal spray coating process: simulations and experiments. Journal of Thermal Spray Technology 11, 206–217.

Shakeri, S, Chandra, S., 2002. Splashing of molten tin droplets on a rough steel surface. International Journal of Heat and Mass Transfer 24, 4561–4575.

Trapaga, G., Szekely, J., 1991. Mathematical modeling of the isothermal impingement of liquid droplets in spraying processes. Metallurgical Transaction B 22, 901–914.

Waldvogel, J.M., Poulikakos, D., 1997. Solidification phenomena in picoliter size solder droplet deposition on a composite substrate. International Journal of Heat Mass Transfer 40, 295–309.

Yang, Z., 2002. Effect of substrate temperature and shape on molten metal droplet impact dynamics, MASc. Thesis, University of Toronto.

Zhao, Z., Poulikakos, D., Fukai, J., 1996. Heat transfer and fluid dynamics during the collision of a liquid droplet on a substrate-I. Modeling. International Journal of Heat and Mass Transfer 39 (13), 2771–2789.

Zheng, L.L., Zhang, H., 2000. An adaptive level set method for moving-boundary problems: application to droplet spreading and solidification. Numerical Heat Transfer Part B 37, 437–454.